JOURNAL OF MATERIALS SCIENCE 29 (1994) 6458–6462

High-temperature creep of yttrium–aluminium garnet single crystals

S. KARATO, Z. WANG, K. FUJINO
Department of Geology and Geophysics, University of Minnesota, Minneapolis, MN 55455, USA

High-temperature creep in single crystals of $Y_3Al_5O_{12}$ (YAG) was studied by constant strain-rate compression tests. The creep resistance of YAG is very high: a stress of ~ 300 MPa is needed to deform at a strain rate of 10^{-6} (s^{-1}) at a temperature as high as 1900 K ($\sim 0.84\ T_m$, (melting temperature)). YAG deforms using the $\langle 1\,1\,1\rangle\ \{1\,\bar{1}\,0\}$ slip systems following a power law with stress exponent $n \sim 3$ and activation energy $E^* \sim 720$ kJ mol^{-1}. However, a small dependence of n on temperature and of E^* on stress was observed. This stress-dependence of activation energy combined with the observed dislocation microstructures suggests that the high creep resistance of YAG is due to the difficulty of dislocation glide as opposed to the difficulty of climb. Present dislocation creep data are compared with diffusion creep data and a deformation mechanism map is constructed. Large transition stresses (2–3 GPa for 10 μm grain size) are predicted. implying that deformation of most fine-grained YAG will occur by diffusion creep.

1. Introduction

High creep resistance of garnets has been well documented [1]. Among the various materials that crystallize into garnet structure, $Y_3Al_5O_{12}$ (YAG) has the highest melting point ($T_m = 2273$ K) and hence is likely to be the most resistant to plastic deformation at high temperatures [2–4]. However, previous studies have several limitations and high-temperature creep in YAG has not been well characterized. The limitations include: (i) very small strains ($< 0.3\%$) in creep tests [3] leading to large uncertainties in creep law parameters, and (ii) the absence of detailed microstructural studies [2–4] causing uncertainties in determining the slip systems and in the interpretation of the mechanical data.

This paper presents a first comprehensive mechanical data set on high-temperature creep of single crystals of YAG together with microstructural observations of deformed specimens using etch pit technique and transmission electron microscopy (TEM). The results are compared with those on other oxide garnets [1, 5] to better understand the deformation mechanisms in single crystals, and also with data on diffusion creep [6] to estimate the relative importance of dislocation and diffusion creep.

2. Materials and methods

A single crystal of Czhokralsky-grown YAG was obtained from MIMports (California); it was ~ 2 cm in diameter and ~ 5 cm long and of more than 99.999% purity. It was oriented using the Laue back reflection technique within 1° to the $\langle 1\,0\,0\rangle$ orientation. Parallelpiped samples ($\sim 2 \times 2 \times 5$ mm^3) were cut from the same single crystals and both ends were polished with a diamond slurry down to 0.3 μm. Compression tests were carried out using an MTS servo-controlled testing machine in air in a $MoSi_2$ furnace. The pistons are made of SiC and the displacement of the specimen was measured using a custom-built *in situ* extensometer by which the relative movement of two sets of SiC rods which touch the bottom of the top piston and the top of the bottom piston respectively, is measured (Fig. 1 [7]). The pistons showed no appreciable deformation up to the maximum temperature (1963 K) and stress (~ 300 MPa) used in this study. However, it was found that YAG reacts with SiC in air at high temperatures, and therefore we inserted corundum (with orientation parallel to the c-axis) in between the YAG and the SiC. To minimize the deformation of corundum, thin discs of YAG were inserted in between the specimens and the corundum platens, which distributes the load on the corundum platens (Fig. 1). The deformation of corundum was found to be significantly less than that of YAG.

In most of the experiments a constant strain-rate (displacement-rate) mode was adopted, in which the change in load (or stress) was measured as a function of strain (time). The strain rate ranged from 0.3×10^{-6} to 4.5×10^{-6} s^{-1}. Temperatures ranged from 1853 to 1963 K ($T/T_m = 0.82$–0.86). The compression tests were made along the $\langle 1\,0\,0\rangle$ orientation. In this orientation, of the two possible types of dislocations [1] those with Burgers vectors $\mathbf{b} = (1/2)\langle 1\,1\,1\rangle$ are activated but those with $\mathbf{b} = \langle 1\,0\,0\rangle$ are not.

After the constant strain-rate tests the specimens were quenched under load and recovered for microstructural observations using an optical microscope

0022–2461

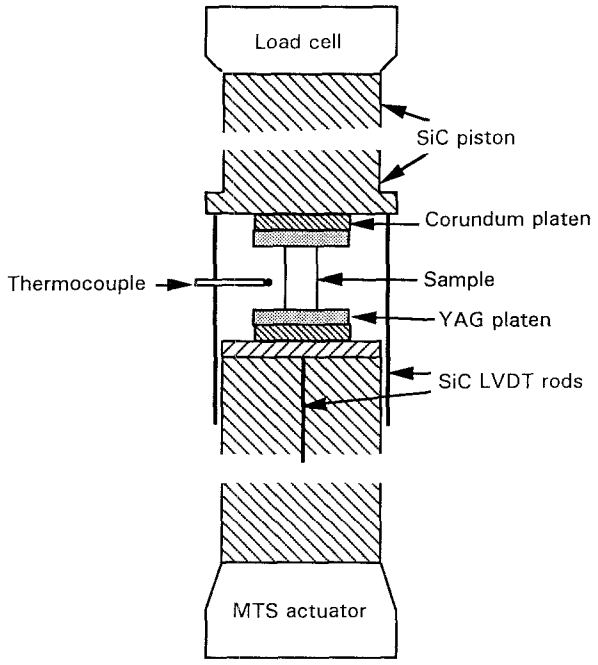

Figure 1 Sample assembly for compression tests.

and a transmission electron microscope (TEM). Etching was made on polished surfaces with H_3PO_4 at 613 K for 3 min to remove the surface layer followed by etching at 523 K for 3 min. Specimens for TEM observations were cut either on or normal to {1 1 0} planes. The TEM specimens were prepared by ion-thinning, and carbon-coated and observed using a Philips CM-30 TEM operated at 300 kV.

3. Results

3.1. Mechanical data

Ductile behaviour was observed only above 1873 K at a strain-rate of $\sim 10^{-6}\,s^{-1}$. Below this temperature all the specimens were fractured at a stress of ~ 350 MPa. When ductile behaviour was observed the stress–strain curves were characterized by marked work hardening followed by quasi steady-state deformation (Fig. 2). A minor peak in stress is observed at relatively low temperatures, but disappears at higher temperatures. Steady-state flow is achieved at ~ 2–4% strain under the test conditions.

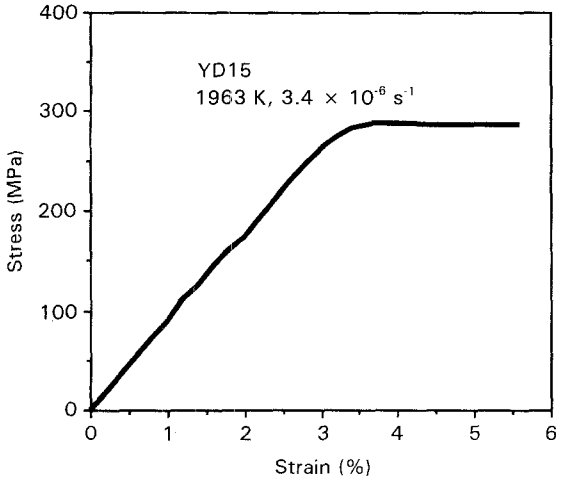

Figure 2 Typical stress–strain curve.

The steady-state data, which are summarized in Table I, were analysed using a power law formula, namely

$$\dot{\varepsilon} = A\sigma^n \exp(-E^*/RT) \quad (1)$$

where $\dot{\varepsilon}$ is strain rate, A is a constant, σ is stress, n is the stress exponent, E^* is activation energy, R is the gas constant and T is absolute temperature. We have determined n and E^* separately from the log (stress) versus log (strain rate) at a given temperature and $1/T$ versus log (strain rate) plot at a given stress respectively (Fig. 3). The results are shown in Fig. 4 and

TABLE I Summary of results with steady-state creep

Run	T (K)	$\dot{\varepsilon}$ ($10^{-6}\,s^{-1}$)	σ (MPa)
YD7-1	1893	0.16	201
YD7-2	1893	0.31	226
YD7-3	1893	0.57	275
YD7-4	1893	0.79	310
YD8	1913	1.48	316
YD9	1913	0.30	189
YD10	1913	0.90	270
YD11	1933	1.37	264
YD12	1933	2.48	324
YD13	1933	0.88	230
YD14	1963	2.51	261
YD15	1963	3.44	294
YD17	1963	4.35	313
YD18	1963	0.75	175
YD19	1893	1.02	328

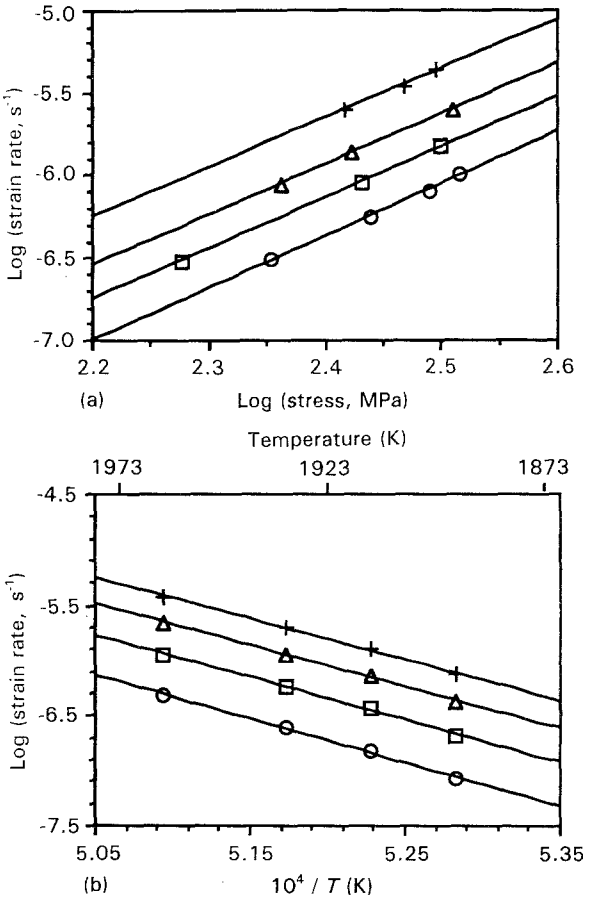

Figure 3 (a) Stress-dependence of strain rate with steady-state creep: ○, 1893 K; □, 1913 K; △, 1933 K and +, 1963 K; (b) temperature-dependence of strain rate with steady-state creep at four typical stresses: ○, 150 MPa; □, 200 MPa; △, 250 MPa and +, 300 MPa.

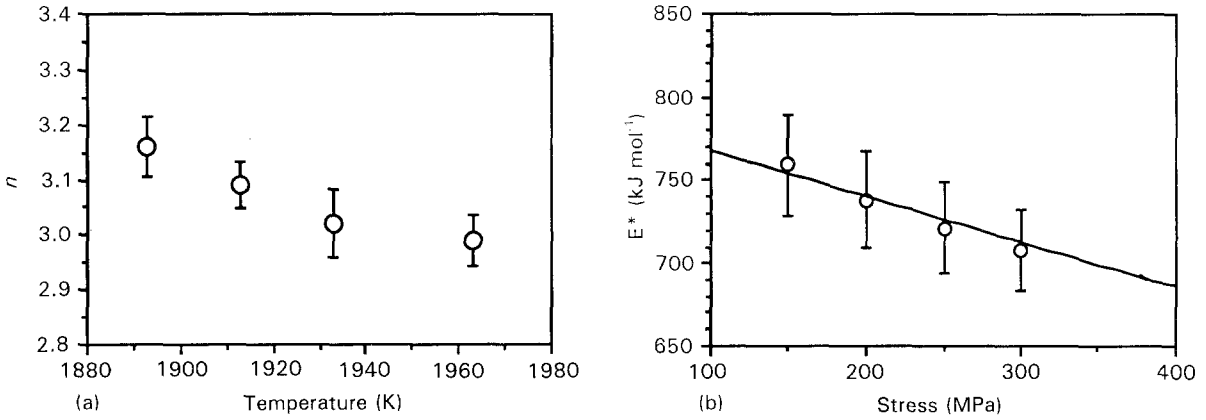

Figure 4 (a) Temperature-dependence of stress exponent; (b) stress-dependence of activation energy.

indicate that both stress exponent and activation energy are not strictly constants. The stress exponent n appears to decrease slightly with temperature (Fig. 4a) and activation energy decreases slightly with stress (Fig. 4b). These observations can be attributed to a dependence of activation energy on stress, namely, $E^* = E_0^* - B\sigma$ with $E_0^* = 803\ \text{kJ mol}^{-1}$ and $B = 0.27$ (kJ mol MPa).

3.2. Microstructural observations

Fig. 5a is a typical optical micrograph of deformed specimens. Well developed conjugate undulatory extinction was observed in specimens deformed under steady-state creep. These extinction bands are interpreted to be the result of lattice distortion due to non-uniform distribution of dislocations and are representative of the trace of glide planes of dislocations. In fact, etch pits observations on polished surfaces (Fig. 5b) show some non-uniform distribution of dislocations, indicating that the dominant slip planes were $\{1\,1\,0\}$.

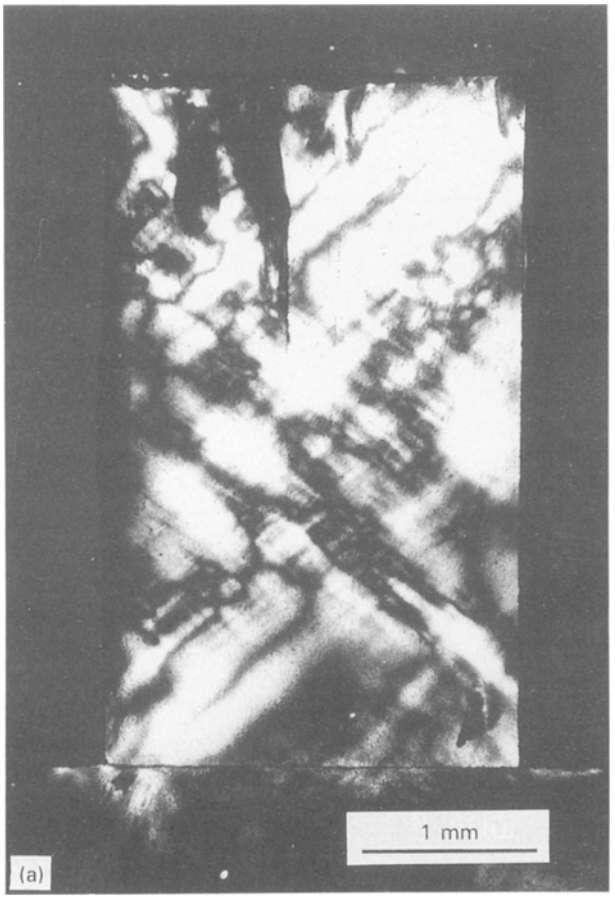

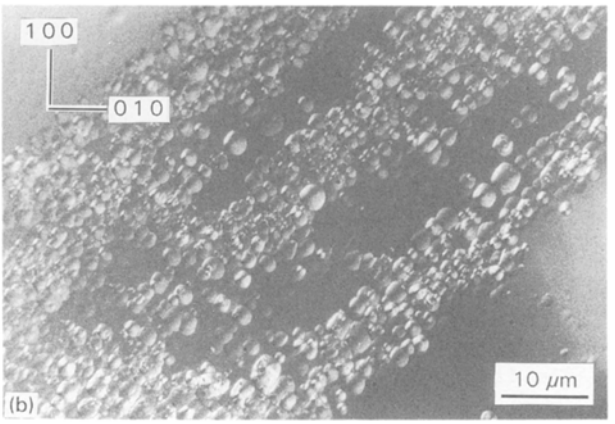

Figure 5 Optical micrographs of a deformed YAG single crystal (YD 15, deformed at $T = 1953$ K, $\dot{\varepsilon} = 3.4 \times 10^{-6}\ \text{s}^{-1}$ to 5.8% strain). Compression axis vertical. (a) Transmitted light with crossed polarizers. Note conjugate slip bands on the $\{1\,1\,0\}$ planes. (b) Etched surface. Note high dislocation density bands on the $(1\,1\,0)$ plane (reflective light with Nomarski contrast).

Dislocation microstructures were also studied using a TEM; a typical dislocation microstructure is shown in Fig. 6. No subgrain boundaries were observed and the distribution of dislocations is uniform when observed in a high-density area shown by etch pits (subboundaries are observed, however, in a specimen annealed at 1963 K for 5 h after deformation). Dislocation configuration is largely similar to that observed in deformed $Gd_3Ga_5O_{12}$ (GGG) [1, 8]: in addition to isolated glide loops, numerous triple junctions are found due to the reactions such as $(1/2)\langle 1\,1\,1\rangle + (1/2)\langle \bar{1}\,\bar{1}\,1\rangle = \langle 0\,0\,1\rangle$ [9]. High-resolution transmission electron microscopy (HRTEM) observations were also made which indicate most of the dislocations have a Burgers vector $\mathbf{b} = (1/2)\langle 1\,1\,1\rangle$. Thus it is concluded that the dominant slip system in YAG for this orientation is $\langle 1\,1\,1\rangle\{1\,\bar{1}\,0\}$.

Overall dislocation densities are rather low: ~ 2–$3 \times 10^{11}\ \text{m}^{-2}$ at stress of ~ 300 MPa, which is about a

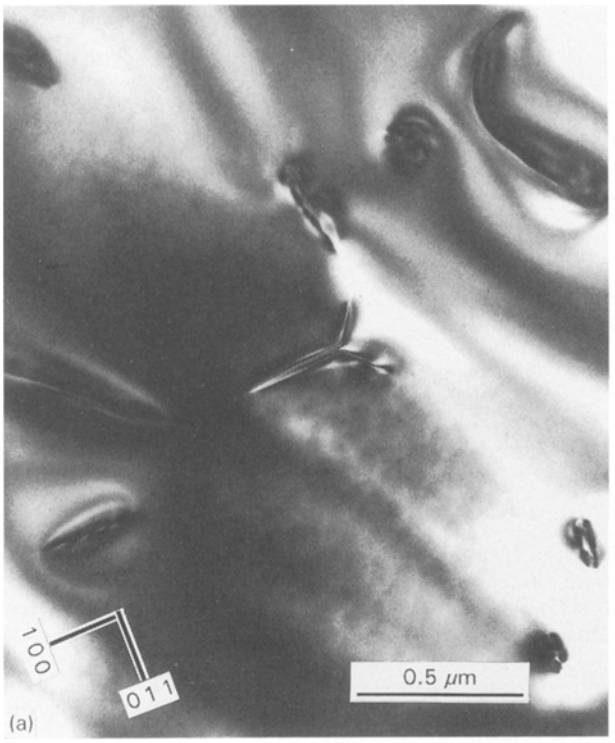

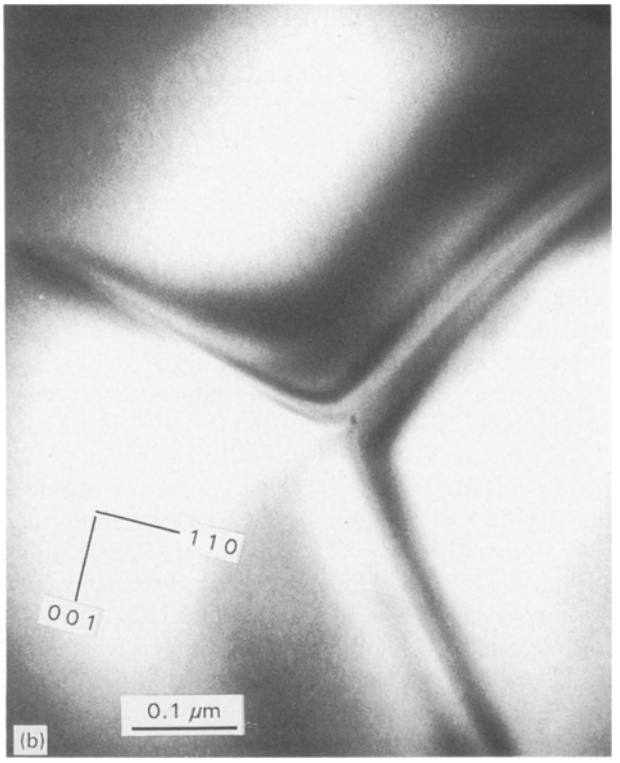

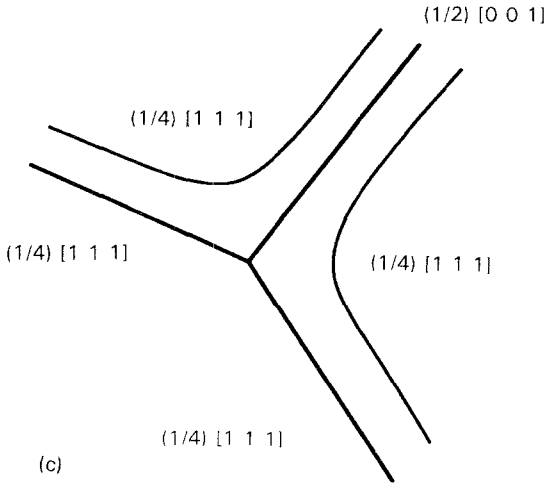

Figure 6 TEMs of a deformed YAG (YD 15, deformed at $T = 1953$ K, $\dot{\varepsilon} = 3.4 \times 10^{-6}\ s^{-1}$ to 5.8% strain). (1 1 0) foil. (a) Typical area showing both isolated glide loops and a triple junction; (b) close-up of a triple junction, showing asymmetrical geometry. An interpretation is shown in (c) which suggests the following dissociation scheme: $[0\,0\,1] = (1/2)[0\,0\,1] + (1/4)[1\,1\,1] + (1/4)[\bar{1}\,\bar{1}\,1]$, $(1/2)[1\,1\,1] = (1/4)[1\,1\,1] + (1/4)[1\,1\,1]$ and $(1/2)[\bar{1}\,\bar{1}\,1] = (1/4)[\bar{1}\,\bar{1}\,1] + (1/4)[\bar{1}\,\bar{1}\,1]$ [9].

factor of 10 smaller than those in other simple oxides (such as MgO) or metals [10]. Similar observations were made in GGG [5] and in some naturally deformed aluminosilicate garnets [11].

4. Discussion

One of the most striking observations is the high creep strength of YAG. The creep strength of YAG and other garnets is higher by a factor of 3–10 than other oxides compared at the same homologous temperatures (T/T_m [12, 13]). Our results are largely consistent with those of Corman [3] (Fig. 7), although the stress exponents are quite different ($n = 6.2$ in Corman [3], whereas it is 3 in the present study). It is believed that this difference is due to the low strains in Corman's experiments, at which creep tests were carried out up to ~0.3% strain. In materials such as garnets where dislocation multiplication is difficult, significant strain-softening is observed [8]. Thus, strain rates measured at small strains tend to underestimate true steady-state strain rates and this tendency will be larger at lower strain rates which leads to a significant overestimation of the stress exponent. In contrast, in our constant strain-rate tests, steady state is more clearly observed in stress–strain curves (Fig. 2).

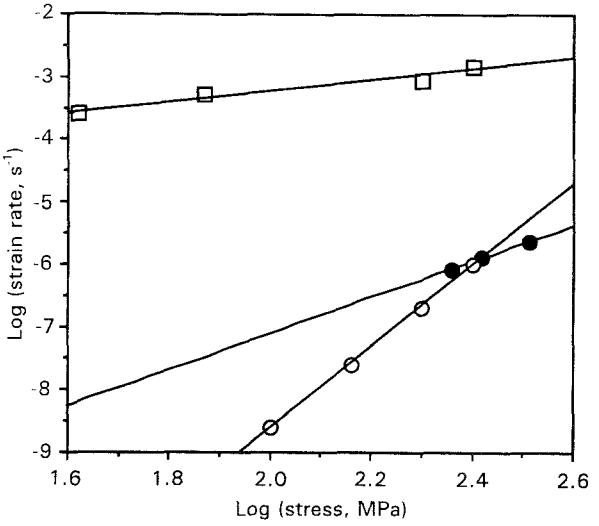

Figure 7 Comparison of ● present results with ○ Corman [3] on single crystals of YAG and with □ Parthasarathy *et al.* [6] on fine-grained (3 μm) polycrystals. $T = 1923$ K.

Garnets in general have two sets of Burgers vectors, namely $\mathbf{b} = \langle 1\,0\,0 \rangle$ and $(1/2)\langle 1\,1\,1 \rangle$. The relation between dominant dislocations and stacking fault energies has been examined theoretically by Rabier *et al.* [9] and a systematic change in dominant Burgers vectors is found in naturally deformed silicate garnets [11]. Rabier *et al.* [9] showed that the geometry of dislocation triple nodes such as shown in Fig. 6b provides useful constraints on dislocation dissociation schemes and the resultant relative role of dislocations with different Burgers vectors. The observed asymmetrical geometry of the triple junction node (Fig. 6b) is consistent with a dislocation dissociation scheme: $[0\,0\,1] = (1/2)[0\,0\,1] + (1/4)[1\,1\,1] + (1/4)[\bar{1}\,\bar{1}\,1]$, $(1/2)[1\,1\,1] = (1/4)[1\,1\,1] + (1/4)[1\,1\,1]$, and $(1/2)[\bar{1}\,\bar{1}\,1] = (1/4)[\bar{1}\,\bar{1}\,1] + (1/4)[\bar{1}\,\bar{1}\,1]$, partial dislocations $(1/4)[1\,1\,1]$ and $(1/4)[\bar{1}\,\bar{1}\,1]$ being common on both sides of the node. This indicates that dislocations with $\mathbf{b} = \langle 1\,0\,0 \rangle$ are more strongly dissociated and less mobile than dislocations with $\mathbf{b} = (1/2)\langle 1\,1\,1 \rangle$. In fact, deformation experiments on GGG (structurally similar to YAG) showed that $\mathbf{b} = (1/2)\langle 1\,1\,1 \rangle$ dislocations are more mobile than $\mathbf{b} = \langle 1\,0\,0 \rangle$ dislocations [5]. This implies that in a polycrystalline material where resolved shear stress is non-zero for both $\mathbf{b} = \langle 1\,0\,0 \rangle$ and $\mathbf{b} = (1/2)\langle 1\,1\,1 \rangle$ dislocations, deformation will occur mostly using $\mathbf{b} = (1/2)\langle 1\,1\,1 \rangle$ dislocations. However, the situation might be different under different deformation conditions as suggested by Ando *et al.* [11].

A common practice in deciphering creep mechanisms is to compare activation energy with that of diffusion. The activation energy of oxygen in YAG is $\sim 310\,\mathrm{kJ\,mol^{-1}}$ [14]. The activation energies of cation diffusion have not been determined, but the experimental data on diffusion creep [6] suggest the activation energy for the slowest diffusing species (probably cations (Y or Al)) is $\sim 580\,\mathrm{kJ\,mol^{-1}}$. In either case, activation energies of diffusion are significantly smaller than that of creep ($\sim 800\,\mathrm{kJ\,mol^{-1}}$ at zero stress). Thus we may rule out simple diffusion-controlled processes such as climb-controlled creep as a rate-limiting process. The observed stress-dependence of activation energy suggests a glide-controlled mechanism of creep [15], and the absence of subboundaries, which are typical in climb-controlled creep [10], also supports this notion. Other supporting evidence for a glide-control model is small internal stress inferred from stress-dip tests [5]. High Peierls stress caused by a large unit cell and the b.c.c. structure [1] is probably responsible for the difficulty of dislocation glide.

The $\langle 1\,1\,1 \rangle\{1\,\bar{1}\,0\}$ slip systems in YAG provide five independent strain components necessary for homogeneous deformation of a polycrystalline aggregate [16]. Therefore the creep strength of an aggregate (with random crystallographic orientation) can be calculated from the creep data for this set of slip systems [17]. The results are compared with diffusion creep data [6] and the transition conditions between diffusion and dislocation creep in polycrystalline aggregates of YAG are calculated. The results are shown in Fig. 8. Since dislocation glide is difficult in YAG but diffusion is not, the conditions under which diffusion creep dominate are rather wide. Under most typical deformation conditions, deformation of polycrystalline YAG will occur by diffusion creep.

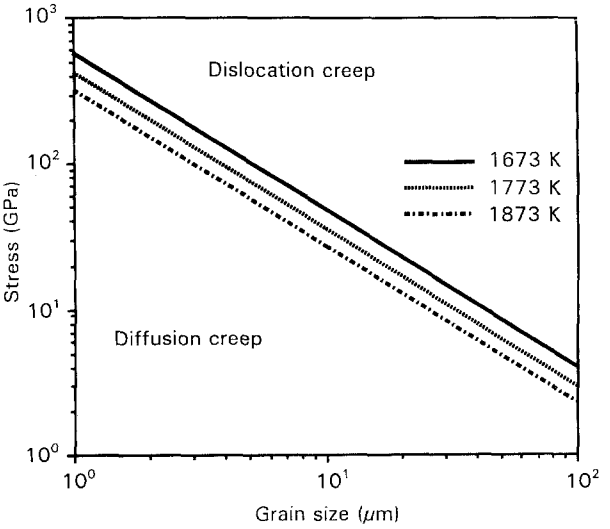

Figure 8 Transition conditions between dislocation and diffusion creep in YAG for several temperatures. Flow law for Nabarro–Herring creep observed in [6] and for dislocation creep determined in this study is used.

Acknowledgement

This work was supported by NSF through grants EAR-9017811 and EAR-9206683.

References

1. J. RABIER and H. GAREM, in "Deformation of Ceramic Materials II", edited by R. E. Tressler and R. C. Bradt (Plenum Press, New York, 1984) pp. 187–198.
2. V. G. GOVOROV, N. N. VOINOVA, KH. S. BAGDASAROV and E. A. STEPANOV, *Sov. Phys. Crystallogr.* **20** (1976) 598.
3. G. S. CORMAN, Final Report on U.S. Air Force Contract No. F33615-87-C-5545, Research and Development Center, General Electric Co., Schenectedy, NY (1990) p. 88.
4. T. A. PARTHASARATHY, T.-I. MAH and L. E. MATSON, *J. Amer. Ceram. Soc.* **76** (1993) 29.
5. Z. WANG, S. KARATO and K. FUJINO, *Phys. Chem. Minerals*, submitted for publication.
6. T. A. PARTHASARATHY, T.-I. MAH and K. KELLER, *J. Amer. Ceram. Soc.* **75** (1992) 1756.
7. C. H. CARTER, Jr., C. A. STONE, R. F. DAVIS and D. R. SCHAUB, *Rev. Sci. Instr.* **51** (1980) 1352.
8. H. GAREM, J. RABIER and P. VEYSSIERE, *J. Mater. Sci.* **17** (1982) 878.
9. J. RABIER, P. VEYSSIERE and J. GRILHE, *Phys. Stat. Sol.* **35** (1976) 259.
10. S. TAKEUCHI and A. S. ARGON, *J. Mater. Sci.* **11** (1976) 1542.
11. J. ANDO, K. FUJINO and T. TAKESHITA, *Phys. Earth Planet. Inter.*, in press.
12. S. KARATO, *ibid.* **55** (1989) 234.
13. S. KARATO, Z. WANG, B. LIU and K. FUJINO, *Earth Planet Sci. Lett.*, submitted for publication.
14. H. HANEDA, Y. MIYAZAKI and S. SHIRASAKI, *J. Cryst. Growth* **68** (1984) 581.
15. H. J. FROST and M. F. ASHBY, "Deformation Mechanism Maps" (Pergamon, Oxford, 1982), p. 168.
16. G. W. GROVES and A. KELLY, *Phil. Mag.* **8** (1963) 877.
17. J. W. HUTCHINSON, *Proc. R. Soc. Lond. A.* **348** (1976) 101.

Received 16 November 1993
and accepted 7 June 1994